Diamond & Related Materials 19 (2010) 1405–1410

Contents lists available at ScienceDirect

Diamond & Related Materials

journal homepage: www.elsevier.com/locate/diamond

High-aspect-ratio, free-form patterning of carbon nanotube forests using micro-electro-discharge machining

Waqas Khalid [1], Mohamed Sultan Mohamed Ali [2], Masoud Dahmardeh, Yongho Choi, Parham Yaghoobi, Alireza Nojeh *, Kenichi Takahata *

Department of Electrical and Computer Engineering, The University of British Columbia, Vancouver BC, V6T 1Z4, Canada

ARTICLE INFO

Article history:
Received 12 May 2010
Received in revised form 9 August 2010
Accepted 12 August 2010
Available online 19 August 2010

Keywords:
Carbon nanotube forests
High-aspect-ratio microstructures
Free-form micromachining
Micro-electro-discharge machining
Chemical vapor deposition
Micro-electro-mechanical systems

ABSTRACT

This paper reports post-growth processing of vertically aligned carbon nanotube forests for the formation of high-aspect-ratio, three-dimensional microstructures in the material. High-frequency pulses of electrical discharge are generated to locally machine the nanotubes in order to create target shapes in a forest. Machining is performed in both dielectric oil and air. The optimal processing is demonstrated in air with a pulse voltage and peak current of 30 V and 60 mA, respectively, providing a discharge gap of ~10 μm. The minimized discharge energy and gap are shown to achieve an aspect ratio of 20 with the smallest feature of 5 μm in forests. Multilayer, three-dimensional geometries with vertical and angled surfaces are successfully obtained without disordering the vertical orientation of the nanotubes. Scanning electron microscopy and energy-dispersive X-ray spectroscopy are used for the surface analysis of the micromachined forests, revealing the dependence of their surface characteristics on the discharge conditions.

1. Introduction

Carbon nanotubes (CNTs) have exceptional mechanical, electrical and optical properties [1–4], which have been utilized to demonstrate various nano-electro-mechanical systems [5–9]. Vertically aligned CNTs (so called CNT forests) are attracting significant attention as they offer unique properties for many applications [10–12]. CNT forests can be viewed as a new type of functional bulk material that can be harvested for numerous applications in micro-electro-mechanical systems (MEMS) and other areas that utilize micromachined structures. For instance, aligned CNTs have been used to create integrated MEMS devices on the wafer scale [13]. Silicon-CNT composite forests have been developed to construct MEMS devices [14]. Microstructured CNT forests are also being utilized in solar cells [15] and fuel cells [16]. The shapes of CNT forests grown by typical chemical vapor deposition (CVD) processes with pre-patterned catalyst [17–19] are, however, primarily limited to two-dimensional-like geometries with a uniform height. In addition, since these forests are grown without any lateral physical support, the dimensional precision of the forest structures tends to degrade as they become tall due to the distortion of the lateral cross-sectional pattern and bending of the structures. Shaping of CNT forests using mechanical molds during growth has been shown [20]. To facilitate the application of this material to MEMS as well as other disciplines, however, it is essential to establish techniques to create high-aspect-ratio, three-dimensional (3-D) microstructures from pre-grown forests. This allows the independent optimization of forest growth and 3-D patterning conditions – other methods (such as the mechanical molding growth), not providing this independence, will be limited in range of structures they can achieve. The chemical and physical stability of CNTs limits the number of effective techniques to pattern the material, which can mainly be enabled by two principles. One involves the use of pulsed lasers to remove CNTs [21,22]. The other technique is micro-electro-discharge machining (μEDM). Pulsed μEDM of carbon nanofibers has been reported in the past [23–25], as well as machining of CNTs using DC arc discharge [26]. However, these studies were only able to show shallow, planar patterns with aspect ratios of <1. Pulsed μEDM was used to machine Polymer-CNT nanocomposites [27]. The composites were made by solution casting and the effect of electrical conductivity on the machinability of the composites was investigated by varying the CNT loading. The present paper reports the first time investigation of high-aspect-ratio, 3-D μEDM of pure CNT forests, providing varying shapes along the height of the forest, unachievable with the conventional CVD growth with pre-patterned catalyst. Microstructure formation with controlled sidewall angles is demonstrated for potential applications to MEMS and other micromachined devices.

2. Experimental preparation and set-up

CNT forest samples used in μEDM experiments were prepared as follows: First, a 10-nm-thick layer of aluminum was evaporated on a

* Corresponding authors. Alireza Nojeh is to be contacted at Tel.: +1 604 827 4346; fax: +1 604 822 5949. Kenichi Takahata Tel.: +1 604 827 4241; fax: +1 604 822 5949.
E-mail addresses: anojeh@ece.ubc.ca (A. Nojeh), takahata@ece.ubc.ca (K. Takahata).
[1] Present address: CoreLabs-Nanofabrication-R&D, King Abdullah University of Science and Technology, Thuwal 23955-6900, Saudi Arabia.
[2] Faculty of Electrical Engineering, Universiti Teknologi Malaysia, Johor 81310, Malaysia.

0925-9635/$ – see front matter © 2010 Elsevier B.V. All rights reserved.
doi:10.1016/j.diamond.2010.08.007

highly-doped silicon wafer (<100>n-type, resistivity 0.008–0.015 Ω cm). Subsequently, a 2-nm-thick layer of iron was deposited. CNT growth was performed in an atmospheric-pressure CVD system. In a typical growth process, after loading the sample, the temperature was ramped up from room temperature to 750 °C in 20 min while maintaining a flow of 500 sccm of hydrogen and 200 sccm of argon in the reaction tube. The sample was then annealed for 3 min under these flow conditions at 750 °C. Subsequently, flow rates of 50 sccm of ethylene, 40 sccm of hydrogen, and 75 sccm of argon were used for 90 min at this temperature for CNT growth, before cooling the samples down to room temperature again. Forests of vertically aligned multi-walled CNTs (as characterized by scanning and transmission electron microscopy) were obtained with lengths of up to several hundreds of micrometers. Various samples with lateral dimensions as large as a few centimeters were grown.

μEDM utilizes pulses of thermomechanical impact induced by a miniaturized electrical discharge generated between a microscopic electrode and a workpiece while, in typical settings, both are immersed in a dielectric liquid [28]. The machining experiments in this effort were performed with a 3-axis μEDM machine (EM203, SmalTec International, USA) that employs relaxation-type resistor-capacitor (*R-C*) circuitry for pulse generation/timing [29]. Fig. 1 illustrates the set-up used for μEDM experiments. Machining voltage is applied so that the electrode serves as the cathode and a CNT forest sample as the anode. To transfer electrical energy stored in the capacitor to pulse generation effectively, it is important to minimize the resistance at electrical contacts in the discharge circuit. For this purpose, the electrical contact to a CNT forest was made by clamping the sample directly on the forest as shown in Fig. 1, which provided a contact resistance of 15–20 Ω. This resistance is much lower than that of 115–1120 Ω measured when the contact is made through the aluminum thin film on the silicon substrate. To machine a CNT forest, a rotating cylindrical electrode of tungsten (at a rotation speed of 3000 rpm) is advanced toward the surface of the forest while the machining voltage is applied between the electrode and the forest. Once a discharge is detected, the feed speed is instantly switched to a selected value to perform the machining process. The tungsten electrode itself is shaped and centered on the rotational axis using a μEDM technique called wire electrical discharge grinding (WEDG) [30]. Several combinations of μEDM parameters were used to optimize the process for 3-D structure formation. Table 1 summarizes the parameters used in the experiments.

3. Results and discussion

μEDM of as-grown CNT forests was performed using a typical machining set-up with kerosene-based dielectric EDM oil (EDM-185 Commonwealth Oil, Canada). The sample was dipped in the oil and μEDM was performed using machining voltage and capacitance in the

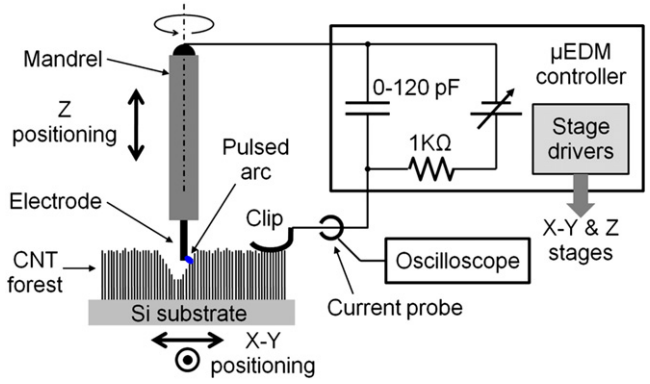

Fig. 1. μEDM setup for CNT forest machining.

Table 1
μEDM conditions used for CNT machining experiments.

Parameter	Values used
Machining voltage (V)	110, 80, 35, 30, 20, 10 or 0 V (0 V for mechanical removal)
Capacitance (pF)	120, 10 or 0
Electrode material	Tungsten
Electrode diameter (μm)	300, 150, 100, or 50
Electrode rotation speed (rpm)	3000 or 0
Feed rate during EDM (mm/min)	*X–Y*: 5, *Z*: 0.5–0.03
Machining environment	Dielectric oil or air

R-C circuit of 80 V and 120 pF, respectively, which are typical values used for conventional μEDM. Several geometries such as holes, slits and squares were patterned, resulting in well-controlled shapes in them. Once the sample dried, however, it was observed that a stress in the CNT forest ripped it apart at areas where the thickness of the CNT forest had been reduced by machining (Fig. 2(a)). The shrinkage/densification of CNT forests by submerging them in liquid has previously been reported to be caused by liquid capillary force [31,32]. To better understand this shrinkage and its relevance to the observed cracks, several pre-patterned CNT forests (cylindrical posts with diameters of a few hundreds of micrometers) that were not processed with EDM were subjected to the dielectric oil used in the EDM process, followed by evaporation/drying (Fig. 2(b)). It can be seen that the forests shrank to almost 1/5th of their original volume, which matches well with the previously reported result [32]. The observed cracks seem to be a purely physical phenomenon related to

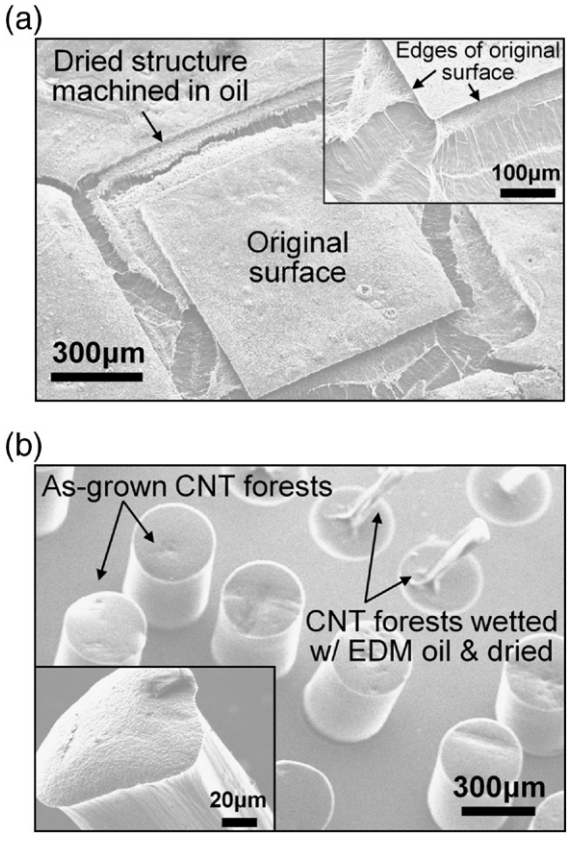

Fig. 2. (a) A square pattern machined in a CNT forest dipped in the dielectric oil and dried. The CNT forest is ripped likely due to the capillary action when the oil evaporated (inset shows a close-up of one of the corners of the square pattern showing the ripped surfaces). (b) Comparison of as-grown cylindrical CNT forests with 300-μm diameter with those dipped in the oil and dried, showing lateral size reduction by about 80% (inset shows a close-up of the tip of a shrunk forest).

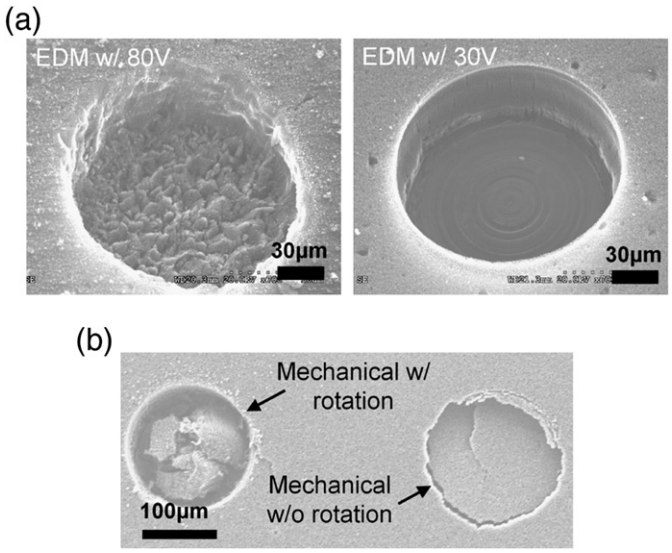

Fig. 3. (a) Hole structures created in a CNT forest using EDM with 80 V and 30 V. (b) Hole structures made by mechanically drilling the forest using the same electrode with and without electrode rotation at 3000 rpm.

this effect induced by the capillary force. Note that this shrinkage may not be a concern for CNT composites (as the space between CNTs is filled with solid material), permitting the use of dielectric oil for their μEDM as implemented for polymer-CNT nanocomposites [27].

In order to avoid the above shrinkage effect in bare CNT forests, experiments were also performed in air. It was observed, however, that processing with the same parameters (80 V, 120 pF) that enabled good patterning and shapes in oil (before drying) caused the local destruction of CNTs with uncontrolled large sparks in air, resulting in non-uniform surfaces and poor sharpness in the structures. The voltage and capacitance were then substantially lowered to 30–35 V and 10 pF, respectively, which produced highly promising results. Fig. 3(a) compares holes drilled at 80 V and 30 V (both with 10 pF) in air, indicating sharper edges and smoother surfaces obtained at 30 V compared with those at 80 V. Note that the bottom of both holes are defined by the tips of CNTs shortened by the machining process. As a control experiment, holes were also created with 0 V, i.e., mechanically drilling the CNT forest, both with and without rotation of the electrode (Fig. 3(b)); it can be seen that the drilled portion is simply dislocated downward and remains within the hole. The results in Fig. 3 thus clearly show the effect of removal by an EDM mechanism.

In order to systematically investigate the effect of voltage on the patterning of CNT forests, experiments were performed using 80, 30, 20 and 10 V with 10 pF as process parameters. Figs. 4(a), (b), and (c) show the contrast when the same pattern (500-μm × 350-μm *X*–*Y* scanning for a depth of 100 μm) was machined with 80, 30 and 10 V, respectively, using a 150-μm-diameter electrode. The forest sample was continuously moved along the rectangle pattern using the *X*–*Y* stage while feeding the electrode until it reached the target depth. It can be seen in Fig 4(a) that machining of CNT forests in air at 80 V led to a distorted structure due to large discharge sparks similar to the result in Fig. 3(a). In contrast, processes with 30 V produced very fine and stable discharge pulses, resulting in well-controlled CNT removal as can be seen in Fig. 4(b). The results with 20 V were similar to those with 30 V. At 10 V, machining exhibited signs of mechanical grinding (Fig. 4(c)). This voltage level at which the mechanical effect starts to be pronounced is found to be much lower than the level (40 V) reported in [23] for pulsed μEDM of carbon nanofibers.

Fig. 5(a) shows a machining process using a 300-μm-diameter cylindrical electrode at 35 V and 10 pF for forming a square pattern in a CNT forest, showing light emission from discharge pulses at the interface between the electrode bottom and the CNT surface. The cubic structure (approximately 200 μm on all sides) in Fig. 5(b) was obtained under these conditions. Fig. 6 shows a typical waveform of a discharge pulse generated at 30 V and 10 pF measured using a current probe (CT-1, Tektronix, Inc., USA) inserted in the discharge circuit as shown in Fig. 1. The measurement result indicates that a pulse with the peak current and pulse duration of approximately 60 mA and 32 ns flows through the CNT forest during the discharge. The peak current is about 1–2 orders of magnitude smaller than those seen in conventional μEDM. This is related to the discharge pulse energy defined by the machining condition, which is expressed as $CV^2/2$, where C is the capacitance of the *R*-*C* circuit and V is the machining voltage, if parasitic capacitances are neglected [28]. With this, a theoretical energy value of 4.5 nJ is calculated with 30 V and 10 pF for machining CNT forests, which is approximately 85 times smaller than that with 80 V and 120 pF, a typical combination used in μEDM of conventional materials.

An important consideration is the gap created between the EDM electrode and the machined structure due to the discharge process, since this gap affects the final dimensions of the structure. In general, smaller gaps are preferred for achieving higher precision and tighter tolerances. The dependence of this gap on the voltage was characterized by measuring the diameter of holes, all of which were drilled using a 100-μm-diameter electrode rotated at 3000 rpm. Fig. 7 plots the average gap distance, G, calculated using the measured diameter of the hole, D_H, and that of the electrode, D_E as $G = (D_H - D_E)/2$, at various voltages. No measurable change in D_E due to the electrode wear was observed ($D_E \cong 100$ μm). The result shows the nonlinear increase of the gap with voltage, and also shows that the gap is around 10 μm at the optimal voltage of 30 V. Note that the effective discharge gap can be smaller than this value as any wobbling of the rotating electrode due to non-idealities in WEDG shaping will make the effective diameter of the electrode during the process larger than D_E. Nevertheless, it can be seen that the measured gaps are smaller by factors of 3–5 than the results reported in [23] if the gaps at the same voltages (60–110 V) are compared. This may be related to a difference in the capacitance used (10 pF plus parasitic capacitance in the present characterization, as opposed to parasitic

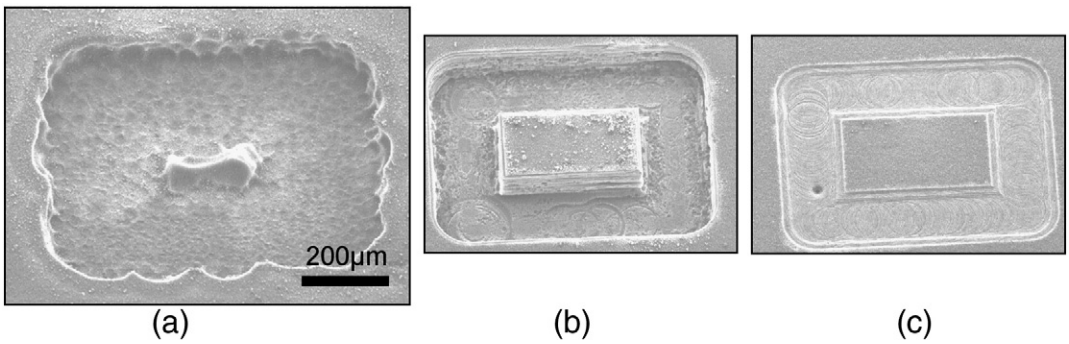

Fig. 4. SEM images with the same magnification showing μEDM results for the same pattern created with (a) 80 V, (b) 30 V, and (c) 10 V.

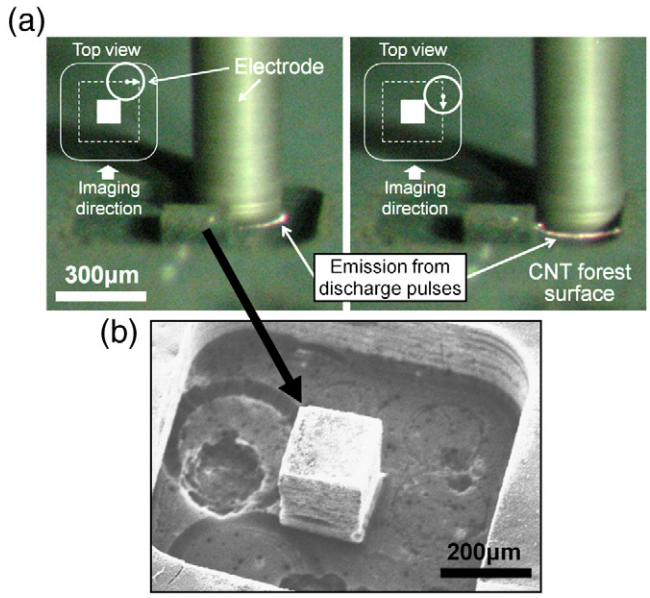

Fig. 5. (a) Optical images during μEDM of a CNT forest. A rotated 300-μm-electrode is scanned along a 500-μm × 500-μm square orbit in the *X*–*Y* plane. The inset in each image shows the top view of the electrode, its orbit (broken line), and the square CNT pattern to be obtained. (b) A 200-μm cube machined in the forest with this process.

capacitance only in the above report), and/or structural differences between the nanofibers involved in the above report and the nanotubes targeted in the present work.

To demonstrate the ability of this technique in 3-D patterning, multi-level, complex micro channels were created in CNT forests. A 50-μm-diameter electrode with 35 V and 10 pF was used to shape the channel structures with depths of 50, 100 and 150 μm (Fig. 8). The 100-μm-deep channel structures achieved a minimum feature size of ~5 μm (Fig. 8(a)), corresponding to an aspect ratio of 20. Even after machining of narrow channel structures, the orientation of aligned nanotubes was intact as can be seen in Fig. 9. The debris on the patterned structures observed after the process (Fig. 8(b)) were easily removed by gently blowing nitrogen onto the sample. The structures in Fig. 8(a) were cleaned by this method; no damage in the structures, including the high-aspect-ratio 5-μm feature, was observed. Another important issue in 3-D patterning is the creation of angled surfaces. This was demonstrated using the electrodes whose shapes were customized by WEDG. Fig. 10(a) shows a pyramid structure machined using an electrode with a cone-shaped tip. The tip of the pyramid has an approximately 38 × 38-μm^2 area and a 130-μm height. The cone-

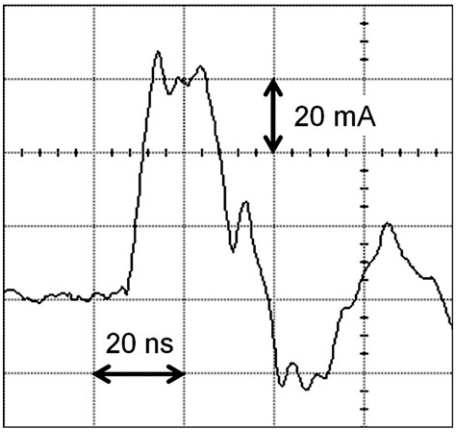

Fig. 6. A sample waveform of discharge pulse observed during CNT machining with 30 V and 10 pF.

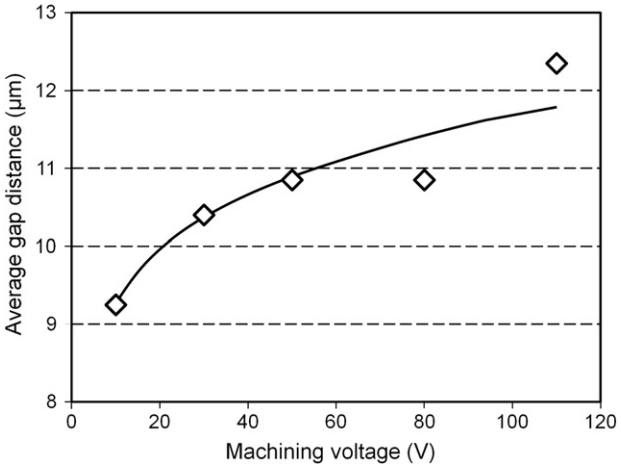

Fig. 7. The electrode-forest gap clearance vs. machining voltage characterized by measuring diameters of holes drilled in a forest using a 100-μm-diameter electrode rotated at 3000 rpm for all data points.

shaped electrode was also used to pattern letters of the alphabet on a CNT forest (Fig. 10(b)). The depths of the letters U, B and C are 120, 150 and 50 μm, respectively. A zoomed view of the middle section of the "B" structure seen in Fig. 10(b) shows sharp edges and smooth, angled surfaces formed in the CNT forest.

Surface analysis of machined forest structures was performed using a scanning electron microscope (SEM) with an energy-dispersive X-ray (EDX) spectroscopic analyzer (Hitachi S-3000 N). The bottom surfaces of 50-μm-deep holes drilled at 30 V and 80 V (both with 10 pF) in the same forest with a height of several hundreds of microns were characterized for this purpose. The EDX analyses (Fig. 11(c)–(e))

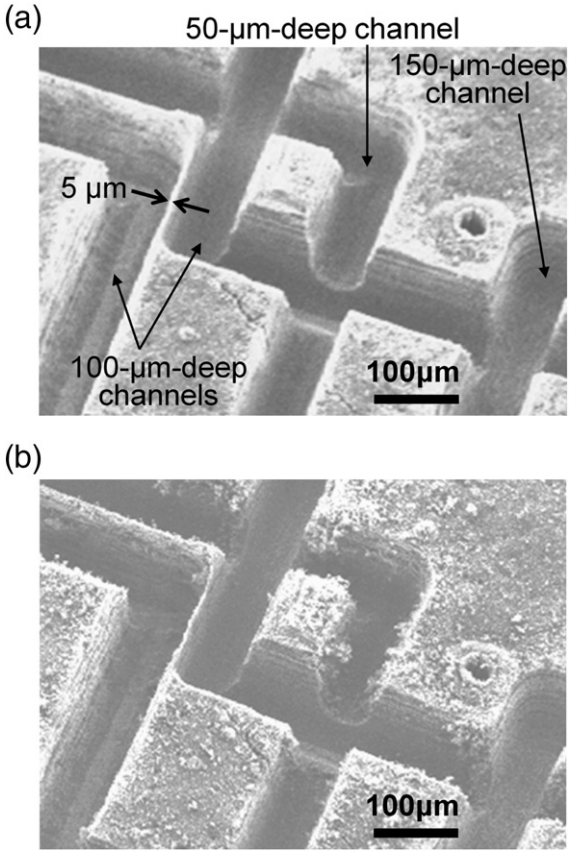

Fig. 8. Multi-level microchannel structures patterned in a CNT forest. (a) The structures after nitrogen cleaning. (b) As-machined structures with debris before cleaning.

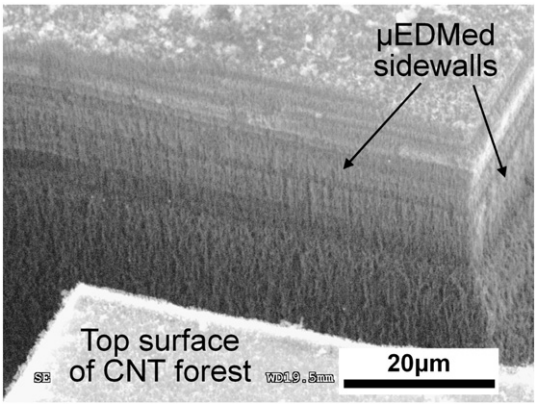

Fig. 9. Sidewalls of a channel created in a CNT forest, showing that the overall vertical orientation of the nanotubes is unaffected by μEDM.

show a high level of silicon in addition to carbon; this is most likely due to the presence of the substrate below the forest. Low levels of catalytic materials (iron was detected but not visible in the plots) as well as oxygen were also detected. At 30 V (Fig. 11(c)), tungsten, the electrode material, was not detected on the surface, suggesting almost zero consumption of the electrode. At 80 V (Fig. 11(b)), the machined surfaces were observed to have submicron-/nanoscale particles. Another EDX focused on the particles revealed that these particles are a compound of tungsten and carbon (Fig. 11(e)). This indicates that at high voltages, the discharge causes some consumption of the electrode at the tip (mainly on the bottom surface, as no measurable diameter change was observed), and tungsten melted from the electrode and carbon removed from the forest are fused to form these particles.

It can be seen in Fig. 11 that the surface processed at 30 V (Fig. 11(a)) is smoother and denser than the surface at 80 V (Fig. 11(b)), which exhibits a texture closer to that of the original forest. This dense surface with 30 V is likely because the carbon removed from the forests tends to remain inside the hole and be spread over the bottom by the rotating electrode when a lower voltage (i.e., lower discharge energy) is used. This hypothesis is supported by the results seen in Fig. 3(a), which shows carbon debris around the hole machined at 80 V but much less particles when 30 V is used. Moreover, the relatively weaker EDX signal of the silicon substrate in the 30-V case (Fig. 11(c)) compared to that in the 80-V case (Fig. 11(d)) can be attributed to the denser surface of the former, as it can attenuate the substrate signal more. The difference in the degree of debris ejection from a machining gap can be related to the magnitude of pressure waves that are caused by thermal expansion of air at the gap induced by discharge pulses, i.e., the smaller the voltage or discharge energy, the lower the ejection pressure hence more debris tend to stay in the hole. Thus, for fine machining with lower energies, debris removal during the process is anticipated to be a key factor for deep or high-aspect-ratio drilling, which will need further investigation. It is worth noting that the situation should be different when the electrode is scanned horizontally, because there are more paths for removed carbon atoms to be ejected from the machining gap compared to the hole-drilling case where the electrode tip is fully enclosed by machined sidewalls of the forest. In fact, the scanned results obtained at 30–35 V in Figs. 4(b) and 8(b) show ejected debris that have been left on the machined structures. This suggests that machining that creates some open space around the electrode may lead to more debris removal from the machining area, which may aid in achieving deeper machining compared to the hole-drilling case.

4. Conclusions

Post-growth 3-D patterning of CNT forests using pulsed μEDM was investigated. A detailed characterization of process parameters was carried out to achieve high-aspect-ratio micromachining of the material. The optimal machining voltage for the process was 20–35 V, which led to a discharge gap of 10 μm. The developed process enabled high-precision formation of 3-D microstructures in CNT forests, almost like regular bulk materials, without the need for lithography and clean-room facilities. The process was demonstrated to provide an aspect ratio of 20 with 5-μm resolution as well as controlled sidewall angles in the machined forest structures. These results suggest that μEDM is a promising technique to promote the application of 3-D CNT forests to MEMS and other micromachined devices and components, e.g., scanning probe arrays, electromechanical switches, microprocessor heat sinks, bio/chemical sensors, superhydrophobic microfluidics, and optical antennas and efficient light capture devices for solar energy applications. The throughput of patterning may be significantly enhanced through batch-mode techniques that use

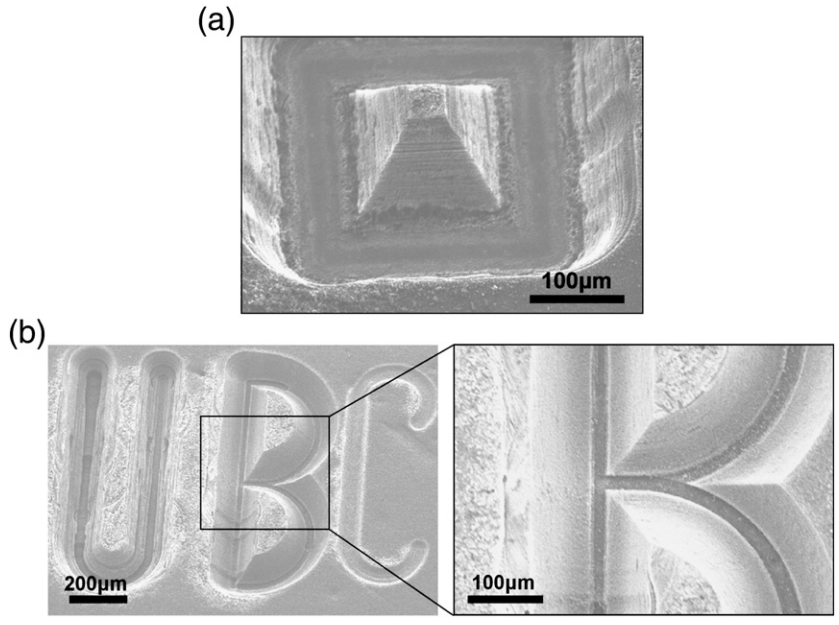

Fig. 10. 3-D μEDM of CNT forests using electrodes with cone-shaped tips performed at 35 V and 10 pF to form (a) a pyramid structure and (b) letters. Note the difference in the depth of the three letters U, B and C.

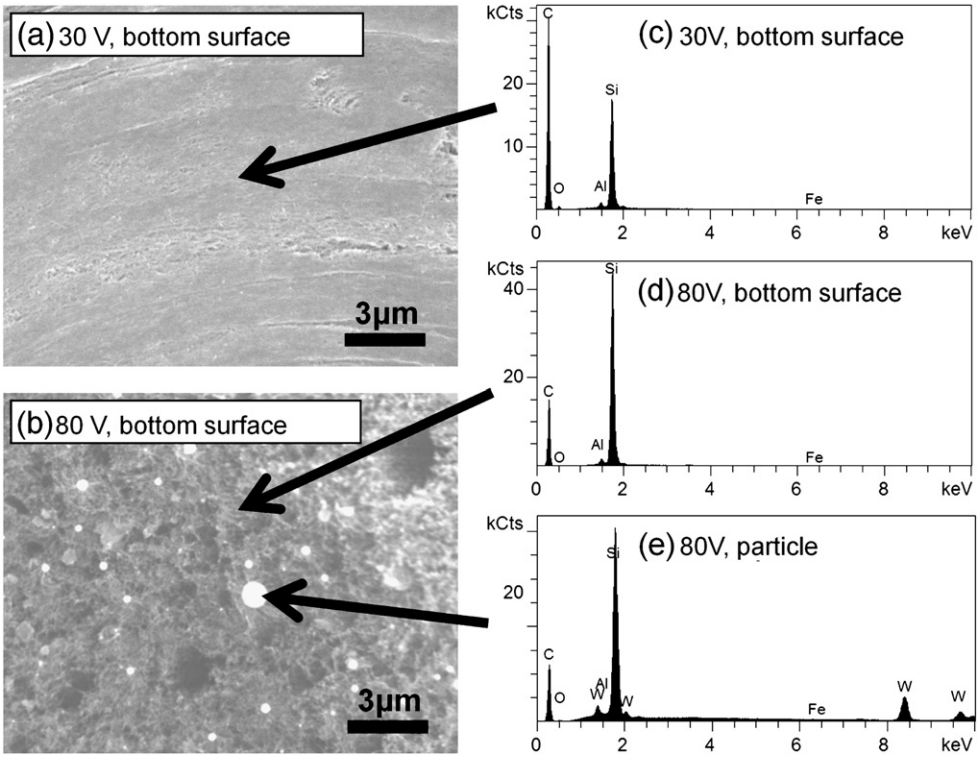

Fig. 11. SEM and EDX results. (a) SEM image of the bottom surface of a hole machined with 30 V in a forest. (b) SEM image of the bottom surface of another hole machined with 80 V in the same forest. (c) EDX analysis of the surface processed at 30 V. (d) EDX analysis of the surface processed at 80 V. (e) EDX analysis of one of the particles observed on the surface processed at 80 V.

arrayed microelectrodes [33]. Future work will involve further optimization of the process along with the evaluation of the impact of the process on nanotube structures and properties.

Acknowledgments

The authors would like to acknowledge the assistance of Mike Chang in CNT forest growth and Greg Wong in preparation of the metal thin films for the growth. This work was partially supported by the Natural Sciences and Engineering Research Council of Canada, the Canada Foundation for Innovation and the British Columbia Knowledge Development Fund.

References

[1] S.S. Samal, S. Bal, J. Miner. Mater. Char. Eng. 7 (2008) 355.
[2] R. Saito, G. Dresselhaus, M.S. Dresselhaus, Physical Properties of Carbon Nanotubes, London Imperial College Press, 1998.
[3] T.W. Odom, J.L. Huang, P. Kim, C.M. Lieber, J. Phys. Chem. B 104 (2000) 2794.
[4] P. Avouris, J. Chen, Mater. Today 9 (1999) 46.
[5] P. Kim, C.M. Lieber, Science 286 (1999) 2148.
[6] R.H. Baughman, C. Cui, A.A. Zakhidov, Z. Iqbal, J.N. Barisci, G.M. Spinks, G.G. Wallace, A. Mazzoldi, D. De Rossi, A.G. Rinzler, Science 284 (1999) 1340.
[7] T.W. Tombler, C. Zhou, L. Alexseyev, J. Kong, H. Dai, L. Liu, C.S. Jayanthi, M. Tang, S.Y. Wu, Nature 405 (2000) 769.
[8] J.E. Jang, S.N. Cha, Y. Choi, G.A.J. Amaratunga, D.J. Kang, D.G. Hasko, J.E. Jung, J.M. Kim, Appl. Phys. Lett. 87 (2005) 163114.
[9] C. Ke, H.D. Espinosa, Small 2 (2006) 1484.
[10] S. Fan, M.G. Chapline, N.R. Franklin, T.W. Tombler, A.M. Cassell, H. Dai, Science 283 (1999) 512.
[11] X. Zhang, K. Jiang, C. Feng, P. Liu, L. Zhang, J. Kong, T. Zhang, Q. Li, S. Fan, Adv. Mater. 18 (2006) 1505.
[12] W.H. Wang, T.H. Hong, C.T. Kuo, Carbon 45 (2007) 97.
[13] Y. Hayamizu, T. Yamada, K. Mizuno, R.C. Davis, D.N. Futaba, M. Yumura, K. Hata, Nat. Nanotechnol. 3 (2008) 289.
[14] D.N. Hutchison, Q. Aten, B. Turner, N. Morrill, L.L. Howell, B.D. Jensen, R.C. Davis, R.R. Vanfleet, Technical Digest of the IEEE International Conference on Solid-State Sensors, Actuators and Microsystems (Transducers) Denver CO, 2009, p. 1604.
[15] R.E. Camacho, A.R. Morgan, M.C. Flores, T.A. McLeod, V.S. Kumsomboone, B.J. Mordecai, R. Bhattacharjea, W. Tong, B.K. Wagner, J.D. Flicker, S.P. Turano, W.J. Ready, J. Miner. Met. Mater. Soc. 59 (2007) 39.
[16] J. Yang, D.J. Liu, Carbon 45 (2007) 2845.
[17] J.J. Sohn, S. Lee, Y.H. Song, S.Y. Choi, K.J. Cho, K.S. Nam, Appl. Phys. Lett. 78 (2001) 901.
[18] K. Hata, D.N. Futaba, K. Mizuno, T. Namai, M. Yumura, S. Iijima, Science 306 (2004) 1362.
[19] A.J. Hart, A.H. Slocum, J. Phys. Chem. B 110 (2006) 8250.
[20] A.J. Hart, H.K. Taylor, A.H. Slocum, Int. J. Nanomanuf. 1 (2007) 701.
[21] K. Kordás, G. Tóth, P. Moilanen, M. Kumpumäki, J. Vähäkangas, A. Uusimäki, R. Vajtai, P.M. Ajayan, Appl. Phys. Lett. 90 (2007) 123105.
[22] W.H. Hung, R. Kumar, A. Bushmaker, S.B. Cronin, M.J. Bronikowski, Appl. Phys. Lett. 91 (2007) 093121.
[23] B.H. Kim, J.G. Ok, Y.H. Kim, C.N. Chu, Ann. CIRP 56 (2007) 233.
[24] J.G. Ok, B.H. Kim, W.Y. Sung, C.N. Chu, Y.H. Kim, Appl. Phys. Lett. 90 (2007) 033117.
[25] J.G. Ok, B.H. Kim, D.K. Chung, W.Y. Sung, S.M. Lee, S. Lee, W.J. Kim, J. Park, C.N. Chu, Y.H. Kim, J. Micromech. Microeng. 18 (2008) 025007.
[26] Y.W. Zhu, C.H. Sow, M.C. Sim, G. Sharma, V. Kripesh, Nanotechnology 18 (2007) 385304.
[27] Y. Wan, D. Kim, Y.B. Park, S.K. Joo, Adv. Compos. Lett. 17 (2008) 115.
[28] T. Masaki, K. Kawata, T. Masuzawa, Proceedings of the IEEE Micro Electro Mechanical Systems, Napa Valley CA, 1990, p. 21.
[29] Y.S. Wong, M. Rahman, H.S. Lim, H. Han, N. Ravi, J. Mater. Process. Technol. 140 (2003) 303.
[30] T. Masuzawa, M. Fujino, K. Kobayashi, T. Suzuki, N. Kinoshita, Ann. CIRP 34 (1985) 431.
[31] N. Chakrapani, B. Wei, A. Carrillo, P.M. Ajayan, R.S. Kane, Proc. Natl Acad. Sci. 101 (2004) 4009.
[32] D.N. Futaba, K. Hata, T. Yamada, T. Hiraoka, Y. Hayamizu, Y. Kakudate, O. Tanaike, H. Hatori, M. Yumura, S. Iijima, Nat. Mater. 5 (2006) 987.
[33] K. Takahata, Y.B. Gianchandani, J. Microelectromech. Syst. 11 (2002) 102.